Félix Zapata, María López-López, José Manuel Amigo, Carmen García-Ruiz. 2018, "Multi-spectral imaging for the estimation of shooting distances", *Forensic Science International*, vol. 282, pp. 80-85.

Available at: DOI: 10.1016/j.forsciint.2017.11.025

Forensic Science International 282 (2018) 80-85

Multi-spectral imaging for the estimation of shooting distances

Félix Zapata[a], María López-López[a], José Manuel Amigo[b,c], Carmen García-Ruiz[a*]

a Department of Analytical Chemistry, Physical Chemistry and Chemical Engineering and University Institute of Research in Police Sciences (IUICP), University of Alcalá, 28871 Alcalá de Henares, Spain

b Department of Fundamental Chemistry, Federal University of Pernambuco, Av. Prof. Moraes Rego, 1235 Cidade Universitária, Recife, Brazil

c Department of Food Science, University of Copenhagen, Rolighedsvej 30, Frederiksberg C, Copenhagen, Denmark

Emails: felix.zapata@uah.es; m.lopezl@uah.es; jmar@food.ku.dk; carmen.gruiz@uah.es

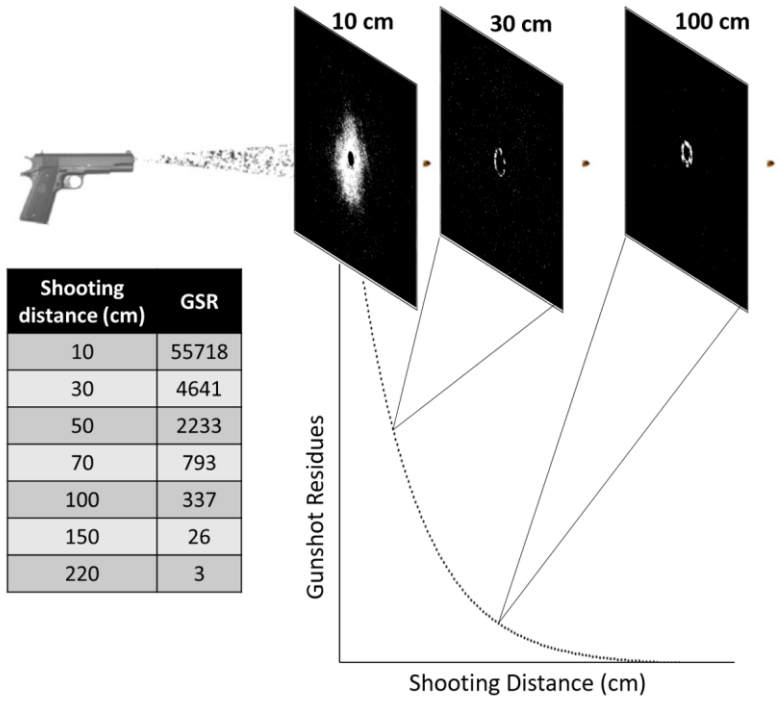

Cite: F. Zapata, M. López-López, J. M. Amigo, C. García-Ruiz, Multi-spectral imaging for the estimation of shooting distances, Forensic Sci. Int. 282 (2018) 80-85. DOI: 10.1016/j.forsciint.2017.11.025

Abstract

Multispectral images of clothing targets shot at seven different distances (from 10 to 220 cm) were recorded at 18 specific wavelengths in the 400–1000 nm range to visualize the gunshot residue (GSR) pattern. Principal component analysis (PCA) showed that the use of violet-blue wavelengths (430, 450 and 470 nm) provided the largest contrast between the GSR particles and the white cotton fabric. Then, the correlation between the amount of GSR particles on clothing targets and the shooting distance was studied. By selecting the blue frame of multispectral images (i.e. the blue frame in the red-green-blue (RGB) system which falls at 470 nm), the number of pixels containing GSR particles was accounted based on the intensity of pixels in that frame. Results demonstrated that the number of pixels containing GSR exponentially decreases with the shooting distance from 30 to 220 cm following a particular exponential equation. However, the targets shot at the shortest distance (10 cm) did not satisfy the above equation, probably due to the noticeable differences of the GSR-pattern of these targets (e.g. high presence of soot). Then, the equation was applied to validation samples to estimate the shooting distances, obtaining results with an error below 10%.

Keywords: Gunshot residues, Multispectral imaging, Image processing, RGB, Shooting distance.

1. Introduction

Significant advances in the visible range of spectroscopy instrumentation such as multi-spectral and hyperspectral imaging systems, make the analysis of large surfaces considerably easy and fast, enabling the discrimination of pixels according to their different visible signatures [1–4]. Furthermore, some applications do not even require the complete visible range, but specific wavelengths that may be selected among the different wave-lengths available in multispectral imaging systems. Multispectral imaging involves the collection of multi-frames (i.e. monocoloured images) of each sample, in which each frame is collected under a specific discrete detection wavelength. In this way, each frame of the image at each wavelength (bidimensional frame, 2D), can be examined separately, or, on the contrary, the whole image comprising all frames (tridimensional image, 3D) can be statistically analysed like hyperspectral images [5]. In fact, the information contained in one or few wavelengths is usually enough to overcome specific challenges in many different fields including food quality control [6–8], cultural heritage [9] or forensics [10–12]. These investigations support the use of multispectral imaging as a fast and relatively inexpensive technique for different forensic purposes. However, no attempts have been made to estimate the shooting distance (muzzle to target distance) by multispectral imaging.

Gunshot residues (GSR), which are produced when a gun is fired, are a complex mixture of burned and unburned particles coming from the propellant, primer components, and metals contained in the projectile (e.g., bullet, bullet jacket, cartridge case) [13–19]. Depending on the firing distance and other conditions (e.g. type of ammunition or firearm, firing angle, atmospheric conditions, etc.), the number of particles that reach the target differs, creating different patterns [13–19]. The forensic analyst estimates the shooting distance through the visual examination of the characteristics of the GSR pattern and, if possible, its comparison to reference GSR patterns (produced under similar conditions) for more accurate results [15–17]. Colour tests based on chemical reactions have been the main method to assist the expert in the visualization of the GSR pattern for decades [14–17].

However, some spectroscopic and imaging techniques have recently demonstrated their efficacy to reveal GSR patterns on clothing [20–23].

The main advantage of using imaging techniques involves the possibility to automatically examine the GSR pattern through quantitative approaches. Up to date, some interesting approaches for shooting distance estimation based on the image analysis of photographed targets through mathematical models have been explored. Most of these mathematical models are calculated taking into account either the amount, number, density, distribution or composition of GSR particles in the target [24–29]. The use of numerical data (besides the GSR pattern) enables to study the mathematical tendency for the variation of GSR pattern with the shooting distance, and the possibility to precisely determine the shooting distance within statistical deviation ranges. On the other hand, quantitative approaches for shooting distance estimation are specially affected by the possible loss of particles due to external factors (blood, water (e.g. rain or washing), first-aid procedures, recovering and handling victim's clothes, etc. [30–32]). Some interesting approaches based on image analysis and mathematical models are, for instance, the estimation of the firing distance performed with a riffle (0–45 cm distances) considering the GSR stained area [25], or the correlation of the density of IR-luminescent GSR particles with shooting distances from 20 to 300 cm performed with different pistols and revolvers [27]. Both studies seem to evidence an exponential decrease in the amount of GSR particles with the shooting distance.

In this respect, this study explores the potential of multispectral imaging as a forensic tool for the visualization of the GSR pattern and the subsequent mathematical estimation of the shooting distance in the 10–220 cm range through a specific exponential equation. To this aim, multispectral images of the clothing targets shot were recorded in the 400–1000 nm range to determine the wavelength that provided the largest contrast between the GSR particles and the white cotton fabric. Then, the correlation between the amount of pixels containing GSR particles and the shooting distance has been mathematically established. Finally, the equation obtained was applied to a set of validation samples.

2. Materials and methods

2.1. Samples

28 square cardboard pieces of 10 × 10 cm covered with standard white cotton clothing were used as targets. White cotton clothing was used in order to enhance the contrast between GSR and background facilitating thereby the visualization of GSR particles. The targets were shot using a Glock G17 pistol and 9 × 19 mm semijacketed hollow point conventional ammunition manufactured by Sellier&Bellot (Czech Republic). Shots were executed at the shooting range of the Spanish National Scientific Police (Madrid, Spain). Targets were shot at seven different shooting distances, including 10, 30, 50, 70, 100, 150 and 220 cm. Four replicates per distance (28 samples) were prepared. Three replicates (21 samples) were used to create the mathematical model whereas a fourth replicate of each distance was used as validation set (7 samples) to test the model.

2.2. Multispectral imaging

A Videometer Lab 4 (Cambridge, UK) was used to collect a multispectral image of each sample at 18 different specific wavelengths from 400 to 1000 nm (430, 450, 470, 505, 565, 590, 630, 645, 660, 700, 850, 870, 890, 910, 920, 940, 950 and 970 nm). Images contained 960 × 1280 pixels, being the spatial resolution of each pixel 0.12 × 0.12 mm.

2.3. Image processing

Image processing was performed in MATLAB R2016b (Mathworks, USA). After comparing the 18 frames of each multispectral image separately, and all together, using principal component analysis (PCA), the frames at violet-blue wavelengths (430, 450 and 470 nm) were identified as the frames that provided the largest contrast between dark GSR and white cotton fabric. As an example, Fig. 1 displays the loading and scores plot for the first principal component of one of the targets shot at 30 cm. According to the loading values and keeping in mind the absolute value, the highest contribution was provided by wavelengths at 430, 450 and 470 nm with 0.50, 0.50 and 0.41, respectively. It should be noted that the contribution of the next wavelength (505 nm) decreases to 0.25 of absolute value. Those 3 violet-blue frames were studied by quantifying the pixels that fall below a specific value of intensity and similar results were obtained for the three frames. From those three, the frame at 470 nm was selected as the most relevant frame because, even though it provided the lowest contribution, it corresponds to the blue channel in commercial ordinary digital RGB cameras. In order to carry out the pixel

quantification, different ranges of intensity were tested, selecting the range from 0 to 0.45 as the optimum range that gave the best correlation with the presence of GSR. It is important to highlight that MATLAB works, by default, with intensity values from 0 (black) to 1 (white) after converting an image into a numerical matrix. Therefore, the dark pixels within this frame were quantified. Afterwards, the image was binarized, i.e. converted only to black and white (only 0/1 values) for image purposes and these values were inverted for better visualization. Finally, the pixel quantification was plotted against the shooting distance (by calculating the average and standard deviation), and different fitting trendlines using the trendline options of Excel (Microsoft Office 2016) and Origin (OriginPro 9.0) were tested by evaluating their R2 coefficient.

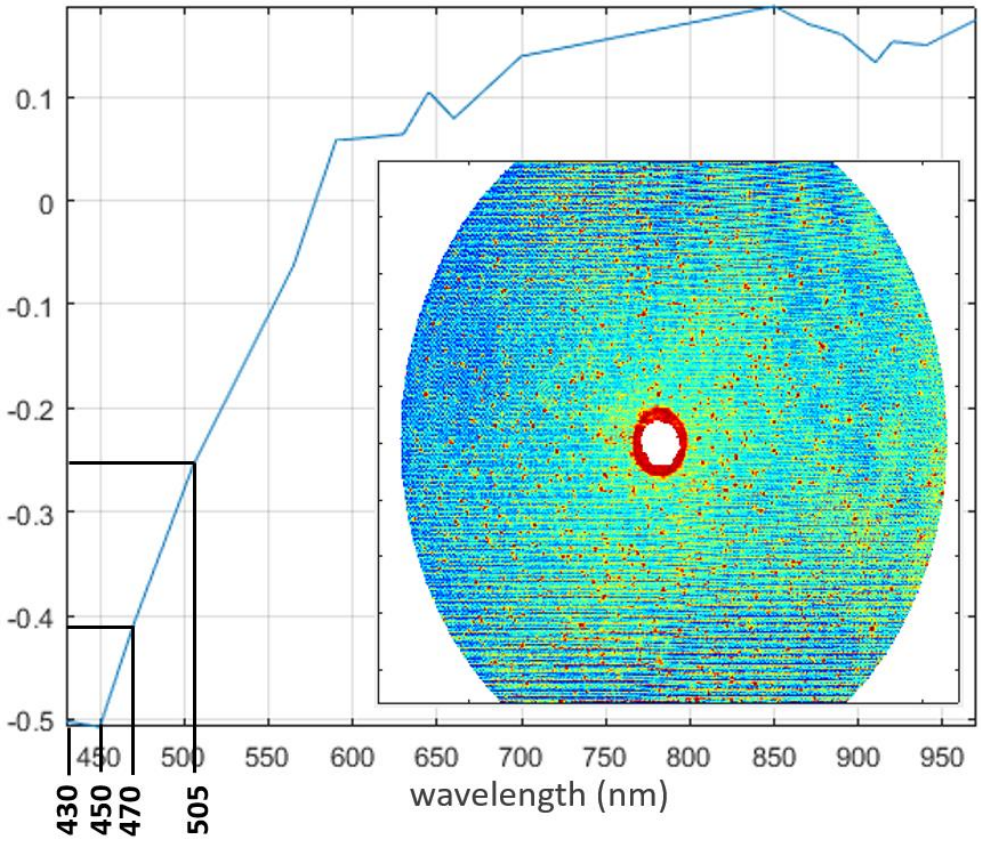

Fig. 1. Graphical loading plot for the first principal component of one of the targets at 30 cm. Principal component analysis using singular value decomposition (svd) algorithm. GSR particles are observed as red dark pixels in the scores image.

3. Results and discussion

First, it is important to highlight that the particles imaged in the white cotton targets exclusively came from the shots, since the shootings were performed under controlled conditions to remove any potential interferent. Also worth noting is the fact that, in this study, the term GSR pattern/GSR particles includes all the particles expelled by the firearm, i.e. particles from both primer and propellant and not only those containing lead-antimony-barium. In fact, most of the GSR particles detected at long distances are propellant particles, as evidenced in previous studies [16,19]. These non-burned or partially burned propellant particles mostly consist of nitrocellulose, the main component in smokeless gunpowders. To avoid confusion, the terms "propellant-GSR particles" and "primer-GSR particles" are used when necessary. The multispectral images obtained for the targets at the different wavelengths in the 400–1000 nm showed that the wavelengths at 430, 450 or 470 nm provided the largest contrast between the GSR particles and the white cotton fabric. However, in order to develop a simple, accessible and broadly usable test for any high-resolution digital camera, the results shown in this study are those from the blue RGB frame at 470 nm. Likewise, no significant improvement was achieved by analysing the whole image (i.e. the 18 frames together) using PCA. Therefore, those results obtained by analysing the blue RGB frames are discussed below. To this aim, Fig. 2(A) displays the images (i.e. blue RGB frame at 470 nm) obtained for the first replicate at 10, 30 and 100 cm distances. By comparing the images, the differences in their GSR pattern are highly recognizable. In fact, an expert eye might estimate an approximate range in the firing distance for each pattern. However, in order to develop a mathematical methodology to support that estimation, the pixels in the image attributed to GSR particles were quantified. The quantification of those pixels in the image that contained GSR was performed through calculating the dark pixels (as previously explained in "Image processing" section). Concretely, different ranges of intensity were tested and it was observed that, beyond the intensity value of 0.45, some pixels of pure cotton started to be accounted besides the GSR. Thus, the optimum range giving the best correlation with the presence of GSR was selected from 0 to 0.45. Afterwards, the image was binarized (only black and white) and inverted (i.e. pixels were interchanged (black ↔ white)) for better visualization. Fig. 2(B) displays the binarized and inverted images for the first replicate shot at 10, 30 and 100 cm distances after selecting only those pixels whose intensity was below 0.45. These images enabled to get a reliable idea of the GSR pattern at each

shooting distance. Furthermore, by this way, those pixels containing GSR can be quantified and correlated to each shooting distance.

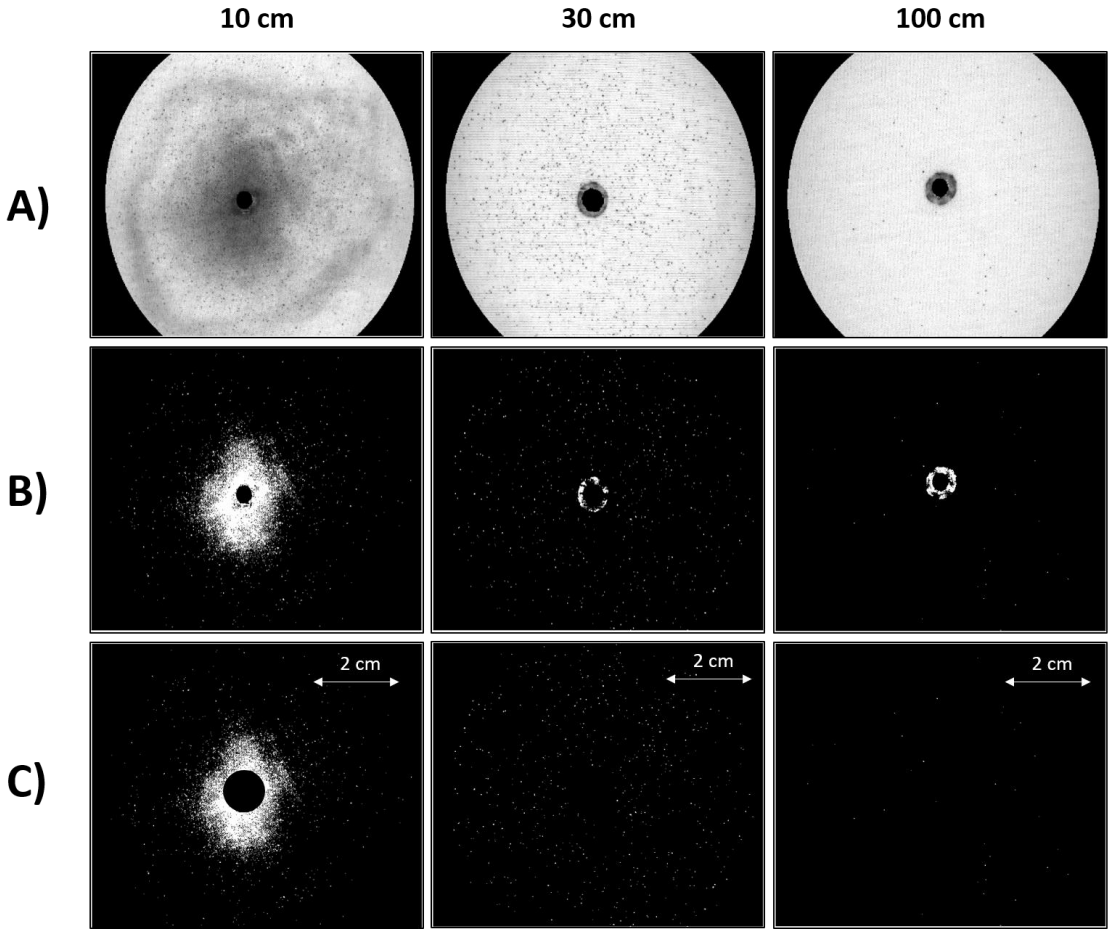

Fig. 2. Grey-scale images of the blue-RGB frames (at 470 nm) of the first replicate at distances 10, 30 and 100 cm after selecting the ROI (A); after inverting and binarizing the pixels containing GSR (B); and after inverting and binarizing the pixels containing GSR removing the bullet wipe and the entrance hole (C).

Regarding the analysis, first, it is important to consider that the residues present on the surface of the bullet were deposited around the immediate margins of the entrance hole as it passed through the clothing. This dark ring, present to a greater or lesser extent in all the targets, does not offer information directly correlated with the shooting distance. For this reason, the area where the bullet wipe residue was present (including the hole) was removed for data treatment. The size of the removed circle-area for all the samples was the maximum-sized bullet wipe residue observed in one of the targets (diameter of 9.5 mm). The results obtained for the images of targets shot at 10, 30 and 100 cm after removing the bullet wipe residue are shown in Fig. 2(C). By comparing these three

images, the decrease in the number of pixels that contain GSR and a higher dispersion with the shooting distance is clearly noticeable.

The GSR amount and dispersion are two main factors that are usually studied to interpret the shooting distance in clothing patterns. Regarding the amount of pixels containing GSR, they were automatically quantified. The results obtained for all distances and replicates are summarized in Table 1.

Table 1. Number of pixels containing GSR for each replicate at the studied shooting distances.

Shooting Distance (cm)	Pixels with GSR Replicate A	Pixels with GSR Replicate B	Pixels with GSR Replicate C
10	58692	63136	45325
30	3864	4509	5551
50	2075	2363	2260
70	797	941	640
100	205	621	184
150	31	18	28
220	1	1	6

It is important to highlight that these values are the number of pixels in the image detected as GSR, not the number of GSR particles itself. In fact, it was observed for all the images that GSR particles varied in size (i.e. the number of pixels each GSR particle covered) by checking the matrix intensity values of the images. There was not a unique size for the GSR particles, but a range of sizes from 1 pixel (the smallest GSR particles) up to 9 pixels (the largest ones). This estimation was made by evaluating the size of those individual particles that reached 150 and 220 cm distance to minimize the possibility of measuring aggregates of particles. Actually, aggregates of these particles would be even bigger.

The number of pixels containing GSR counted for each replicate (Table 1) were plotted against the shooting distance after calculating the average and standard deviation. The resultant graphic could poorly fit both a power ($y = 2 \times 10^8\ x^{-3.051}$) and an exponential equation ($y = 27984\ e^{-0.044x}$) with coefficients of determination (R-squared) of 0.921 and 0.967, respectively. By considering these two fittings, it was noticed that the number of pixels containing GSR at 10 cm shooting distance was lower than those expected for a power equation but higher than those expected for an exponential equation. By visually comparing the targets at 10 cm with the targets at the other distances, the differences are noticeable. The 10 cm-targets evidenced the presence of defined GSR particles also

present in the targets at the other shooting distances (organic propellant-GSR particles); and a dark continuous diffuse region stained by smaller (microscopic) particles (probably soot and inorganic lead-based GSR particles) that was not present in the other targets. As previously indicated, the size of propellant-GSR particles varied from 1 pixel (the smallest particles detected) to 9 (3 × 3) pixels (the largest ones). Since one pixel is 120 mm (the resolution of the camera), the approximate size range for the particles detected was 100–400 μm diameter. Thus, a limit of detection of approximately 100 μm of particle diameter is estimated for this camera. The size of carbon black particles that formed the soot is known to be in the order of nanometres [33]. The size of inorganic primer-GSR particles are known to be in the order of microns, concretely, within the range 0–30 μm (>10 μm when forming aggregates) [14,19]. This implies that no individual carbon or primer-GSR particles (or even aggregates of them) are being detected with this camera, except when a huge number of them densely covers a specific area, as occurs for 10 cm-shooting distance. This evidences a highly steep decrease of carbon black and primer-GSR particles with the shooting distance since these particles massively reached only the closest targets placed at 10 cm distance. This result is in accordance with previous studies [16,19,32] which reported that "at intermediate-long distances, between 0.75 and 3 m depending on the ammunition and the weapon type used, very few microscopic inorganic GSR particles usually deposit on the target" [16].

The reason for the steeper decrease of these microscopic particles is not clear. One possibility involves a different flight behaviour for carbon-black and primer-GSR particles with respect to propellant-GSR particles as a consequence of their different air resistance, explained by their significantly different weight, shape and size. As evidenced in literature, the shooting distance that particles reach strongly depends on their air resistance (influenced by factors such as their morphology) [30]. Nevertheless, further investigations on this issue are required to confirm this hypothesis.

In any event, the huge amount of primer-GSR particles at very short distances leads to an over-count of the pixels containing GSR for the 10 cm-targets in comparison to the other shooting distances, providing larger numbers of pixels containing GSR than those expected using an exponential equation.

Taking this into account, a graph in which the 10 cm targets were removed, was plotted (Fig. 3). This graph properly fits an exponential equation (R-squared = 0.994).

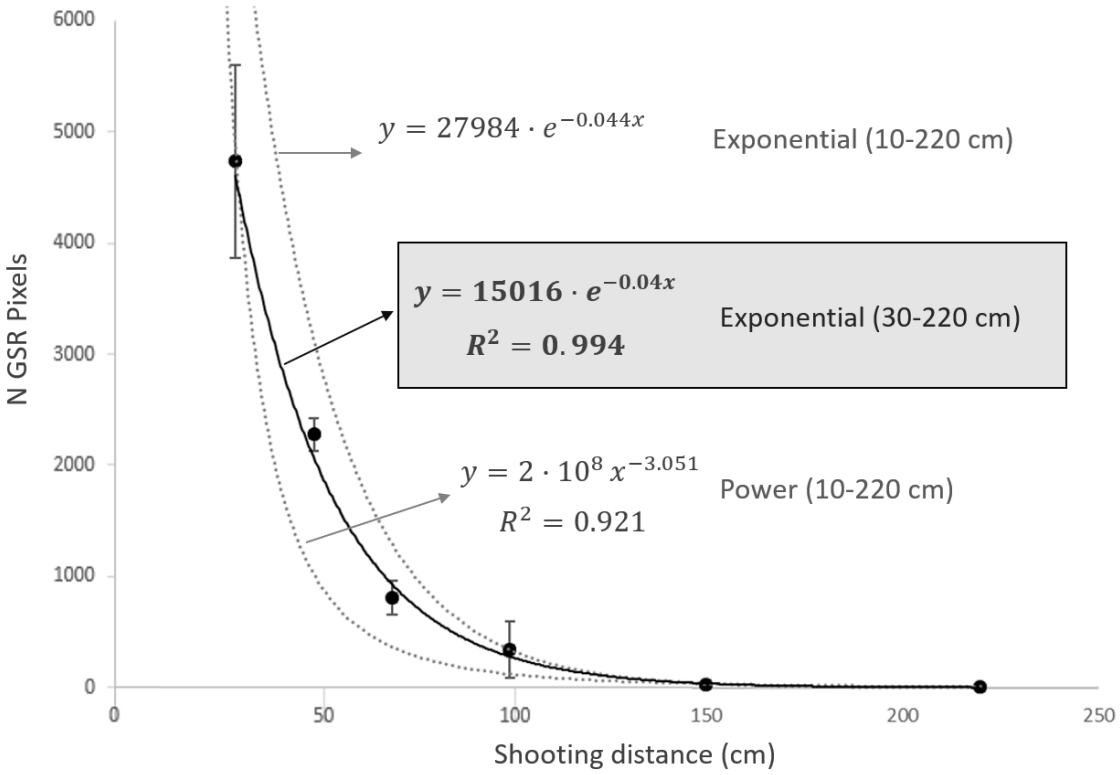

Fig. 3. Graphical plot: number of pixels containing GSR against the shooting distance from 30 to 220 cm. The best exponential fitting for 30–220 cm is shown as a black solid line. The power and exponential fittings for 10–220 cm (previously calculated) are also displayed as grey dotted lines for comparison purposes.

The number of pixels that contain GSR exponentially decreases with the shooting distance within the range from 30 to 220 cm, following the equation:

$$Number\ of\ pixels\ containing\ GSR = 15016e^{-0.04(shooting\ distance\ in\ cm)}$$

Operating to find the shooting distance:

$$Shooting\ distance\ (cm) = ln(15016/Number\ of\ pixels\ containing\ GSR)/0.04$$

Therefore, according to this result: (i) the total amount of GSR correlates with the shooting distance through a specific exponential equation (from 30 to 220 cm), in such a way that the distance might be estimated from the amount of pixels containing GSR; and (ii) for a shooting distance of 220 cm, the amount of GSR is almost zero. Therefore, the

detection of no pixels containing GSR would imply a shooting distance larger than 220 cm for this gun and ammunition type.

This hypothesis was tested by interpolating the amount of pixels containing GSR from the fourth replicate of each distance, whose results are summarized in Table 2.

Table 2. Shooting distances calculated by interpolating the results obtained for the fourth replicate of each shooting distance (pixels containing GSR) into the exponential equation.

Real distance (cm)	Pixels with GSR 4th replicate	Estimated distance	Relative Error (%)	Determined distance range considering the standard deviation (cm)
30	4995	27.5	-8.3	23.6-32.2
50	2072	49.5	-1.0	47.8-51.3
70	793	73.5	5.0	69.2-78.8
100	301	97.7	-2.3	82.8-140.5
150	25	159.9	6.6	153.9-167.9
220	1	240.4	9.3	> 206.5

According to the obtained results, the estimated distance was always determined with a relative error below 10% within the whole range of distances 30–220 cm. Moreover, the standard deviation of the model (i.e. from the 3 replicates used to create the model) might be taken into account by providing a range of shooting distances in the results obtained for the validation samples. Positively, the real shooting distance was always included in the interpolated range except for one of the distances (150 cm).

4. Conclusions

Targets shot from seven different distances (10–220 cm) with conventional ammunition were analysed using multispectral imaging within the range 400–1000 nm. The acquisition taken at 430, 450 and 470 nm wavelengths provided the largest contrast between the dark GSR particles and white cotton fabric.

The amount of pixels containing GSR particles was calculated based on the greyscale intensity of pixels in the blue RGB frame, at 470 nm. Results showed an exponential decrease in the amount of pixels containing GSR with the shooting distance. This exponential decrease properly fits the specific equation (*Number of pixels containing GSR* $= 15016e^{-0.04(\text{shooting distance})}$) for shooting distances between 30 to 220 cm.

In addition, the results obtained in this study indicated that the non-detection of GSR particles in the images would involve a shooting distance longer than 220 cm for the ammunition, weapon, and conditions used. On the other hand, the quantification of an excessive number of pixels (that may even exceed the estimations made by the exponential equation) would imply a shooting distance within the range 0–30 cm. This is due to the different GSR pattern, observed for very short shooting distances, which contained a grey diffuse region (attributed to carbon black and primer-GSR particles), that considerably increased the number of pixels containing GSR over the estimation provided by the exponential equation. Thus, further studies evaluating additional shooting distances within the range 0–30 cm should be performed in order to find a more accurate mathematical equation applicable to very short-range distances.

Finally, it is important to highlight that favourable and known conditions (i.e. ammunition type, gun, white cotton as background, shots performed in a shooting gallery, perpendicular shots to targets, evidence recovery just after shooting, no blood, water or dust contamination, etc.) were employed in this research, due to its preliminary nature. Thus, its immediate application to real casework is, nowadays, unfeasible. How the correlation curve is affected by all these factors needs to be evaluated and think solutions to overcome such problems when estimating the shooting distance in real samples.

Acknowledgements

The authors thank the Spanish Ministry of Education for the project MINECO-CTQ2014-58688-R. The authors also thank the support of police for preparing the samples. Félix Zapata also thanks the Spanish Ministry of Education for his PhD research fellowship FPU014/00790.

References

[1] C. Chang, Hyperspectral Imaging: Techniques for Spectral Detection and Classification, USA Plenum Publishers, New York, 2003.

[2] H.F. Grahn, P. Geladi, Techniques and Applications of Hyperspectral Image Analysis, Wiley, Great Britain, 2007.

[3] B.E. Bernacki, T.A. Blake, A. Mendoza, T.J. Johnson, Visible hyperspectral imaging for standoff detection of explosives on surfaces, Proc. SPIE 7838 (2010) 78380C/1–78381C/7.

[4] G.J. Edelman, E. Gaston, T.G. van Leeuwen, P.J. Cullen, M.C.G. Aalders, Hyperspectral imaging for non-contact analysis of forensic traces, Forensic Sci. Int. 223 (2012) 28–39.

[5] J.M. Amigo, H. Babamoradi, S. Elcoroaristizabal, Hyperspectral image analysis. A tutorial, Anal. Chim. Acta 896 (2015) 34–51.

[6] J. Li, L. Chen, W. Huang, Q. Wang, B. Zhang, X. Tian, S. Fan, B. Li, Multispectral detection of skin defects of bi-colored peaches based on vis-NIR hyperspectral imaging, Postharvest Biol. Technol. 112 (2016) 121–133.

[7] J.C. Noordam, W.H. Van Den Broek, L.M.C. Buydens, Detection and classification of latent defects and diseases on raw French fries with multispectral imaging, J. Sci. Food Agric. 85 (2005) 2249–2259.

[8] J. Liu, Y. Cao, Q. Wang, W. Pan, F. Ma, C. Liu, W. Chen, J. Yang, L. Zheng, Rapid and non-destructive identification of water-injected beef samples using multispectral imaging analysis, Food Chem. 190 (2016) 938–943.

[9] E. Marengo, M. Manfredi, O. Zerbinati, E. Robotti, E. Mazzucco, F. Gosetti, G. Bearman, F. France, P. Shor, Technique based on LED multispectral imaging and multivariate analysis for monitoring the conservation state of the Dead Sea Scrolls, Anal. Chem. 83 (2011) 6609–6618.

[10] L. Caneve, F. Colao, M. Del Franco, A. Palucci, M. Pistilli, V. Spizzichino, Multispectral imaging system based on laser induced fluorescence for security applications, Proc. SPIE 9995 (2016) 999508/1–999508/7.

[11] H. Östmark, M. Nordberg, T.E. Carlsson, Stand-off detection of explosives particles by multispectral imaging Raman spectroscopy, Appl. Opt. 50 (28) (2011) 5592–5599.

[12] Z. Khan, F. Shafait, A. Mian, Automatic ink mismatch detection for forensic document analysis, Pattern Recogn. 48 (2015) 3615–3626.

[13] M. López-López, C. García-Ruiz, Recent non-chemical approaches to estimate the shooting distance, Forensic Sci. Int. 239 (2014) 79–85.

[14] F.S. Romolo, P. Margot, Identification of gunshot residue: a critical review, Forensic Sci. Int. 119 (2001) 195–211.

[15] A. Zeichner, B. Glattstein, Recent developments in the methods of estimating shooting distance, Sci. World J. 2 (2002) 573–585.

[16] D. Muller, A. Levy, A. Vinokurov, M. Ravreby, R. Shelef, E. Wolf, B. Eldar, B. Glattstein, A novel method for the analysis of discharged smokeless powder residues, J. Forensic Sci. 52 (2007) 75–78.

[17] O. Dalby, D. Butler, J.W. Birkett, Analysis of gunshot residue and associated materials—a review, J. Forensic Sci. 55 (2010) 924–943.

[18] M. López-López, C. Alvarez-Llamas, J. Pisonero, C. García-Ruiz, N. Bordel, An exploratory study of the potential of LIBS for visualizing gunshot residue patterns, Forensic Sci. Int. 273 (2017) 124–131.

[19] Z. Brozek-Mucha, Scanning electron microscopy and X-ray microanalysis for chemical and morphological characterisation of the inorganic component of gunshot residue: selected problems, Biomed. Res. Int. (2014) 1–11, doi:http://dx.doi.org/10.1155/2014/428038.

[20] C.S. Atwater, M.E. Durina, J.P. Durina, R.D. Blackledge, Visualization of gunshot residue patterns on dark clothing, J. Forensic Sci. 51 (2006) 1091–1095.

[21] J.A. Bailey, Digital infrared photography to develop GSR patterns, Aust. J. Forensic Sci. 39 (2007) 33–40.

[22] H. Brown, D.M. Cauchi, J.L. Holden, H. Wrobel, S. Cordner, Image analysis of gunshot residue on entry wounds I—the technique and preliminary study, Forensic Sci. Int. 100 (1999) 163–177.

[23] H. Tugcu, C. Yorulmaz, Y. Karslioglu, H.B. Uner, S. Koc, C. Ozdemir, A. Ozaslan, B. Celasun, Image analysis as an adjunct to sodium rhodizonate test in the evaluation of gunshot residues, Am. J. Forensic Med. Pathol. 27 (2006) 296-299.

[24] W. Lichtenberg, Methods for determination of shooting distance, Forensic Sci. Rev. 2 (1) (1990) 37–62.

[25] H. Brown, D.M. Cauchi, J.L. Holden, H. Wrobel, S. Cordner, Image analysis of gunshot residue on entry wounds II—a statistical estimation of firing range, Forensic Sci. Int. 100 (1999) 179–186.

[26] A. Biedermann, F. Taroni, A probabilistic approach to the joint evaluation of firearm evidence and gunshot residues, Forensic Sci. Int. 163 (2006) 18–33.

[27] R. Hofer, S. Graf, S. Christen, The use of unburned propellant powder for shooting distance determination. Part 1: infrared luminiscence, Forensic Sci. Int. 273 (2017) 10–19.

[28] R. Hofer, P. Wyss, The use of unburned propellant powder for shooting distance determination. Part 2: diphenylamine reaction, Forensic Sci. Int. 278 (2017) 24–31.

[29] Z. Brozek-Mucha, Distribution and properties of gunshot residue originating from Luger 9 mm ammunition in the vicinity of the shooting gun, Forensic Sci. Int. 183 (2009) 33–44.

[30] M. Bonfanti, A. Gallusser, Problems encountered in the detection of gunshot residues, AFTE J. 27 (2) (1995) 105–121.

[31] A. Vinokurov, A. Zeichner, B. Glattstein, A. Koffman, N. Levin, A. Rosengarten, Machine washing or brushing of clothing and its influence on shooting distance estimation, J. Forensic Sci. 46 (6) (2001) 928–933.

[32] A. Vinokurov, A. Zelkowicz, E. Wolf, A. Zeichner, The influence of a possible contamination of the victim's clothing by gunpowder residue on the estimation of shooting distance, Forensic Sci. Int. 194 (2010) 72–76.

[33] J.B. Donnet, R.C. Bansal, M.J. Wang, Carbon Black: Science and Technology, second edition, revised and expanded, CRC Press, New York, 1993.